Generic equilibration dynamics of planar defects in trapped atomic superfluids

Peter Scherpelz, Karmela Padavić, Andy Murray, Andreas Glatz, Igor S. Aranson, and K. Levin

Generic equilibration dynamics of planar defects in trapped atomic superfluids

Peter Scherpelz,[1] Karmela Padavić,[1] Andy Murray,[1] Andreas Glatz,[2, 3] Igor S. Aranson,[2] and K. Levin[1]

[1] *James Franck Institute and Department of Physics,*
University of Chicago, Chicago, Illinois 60637, USA
[2] *Materials Science Division, Argonne National Laboratory,*
9700 South Cass Avenue, Argonne, Illinois 60439, USA
[3] *Department of Physics, Northern Illinois University, DeKalb, Illinois 60115, USA*

We investigate equilibration processes shortly after sudden perturbations are applied to ultracold trapped superfluids. We show the similarity of phase imprinting and localized density depletion perturbations, both of which initially are found to produce "phase walls". These planar defects are associated with a sharp gradient in the phase. Importantly they relax following a quite general sequence. Our studies, based on simulations of the complex time-dependent Ginzburg-Landau equation, address the challenge posed by these experiments: how a superfluid eventually eliminates a spatially extended planar defect. The processes involved are necessarily more complex than equilibration involving simpler line vortices. An essential mechanism for relaxation involves repeated formation and loss of vortex rings near the trap edge.

I. INTRODUCTION

Our understanding of superfluid equilibration has been greatly enhanced by research in trapped ultracold atomic gases. In contrast to condensed matter systems, here there is flexibility in engineering a highly controlled perturbation, as well as the capability of studying the ensuing relaxation processes in real time experiments. Such studies inform about the nature of non-equilibrium superfluid dynamics and equilibration processes. Of particular interest are the nature of defects formed by perturbations, and the life cycle of these defects as they equilibrate. In this paper we focus on extended planar defects in two and three dimensions and establish (from both numerical observation and analytical arguments) the processes whereby these evolve during equilibration. We point out that these planar defects which we call "phase walls" (as in "domain walls"– surfaces along which there is a sharp gradient of the phase) are rather ubiquitous; they undergo a reproducible evolutionary sequence towards a simpler defect, as for example a single line vortex. In contrast to line vortices which tend to precess within the trap before exiting, the healing processes of these more extended defects are quite complex.

Indeed, it is not obvious how even a commonly-studied planar defect, a dark soliton (a planar density depletion, stable in 1D and associated with a phase shift) eventually decays in realistic 2D or 3D traps, as it must. What we show here is that the decay of extended planar defects involves vortex rings. But these rings are not the end-product of a process in which the plane disappears, nor are they in general associated with a "soliton-ring oscillation" process [1]. Rather there is a co-existence of phase wall with near-trap-edge vortex rings which repeatedly enter and exit the trap.

Our work is based on simulations and analysis of two types of experiments which give rise to planar defects. These include applying localized depletions of density or alternatively subjecting the system to phase-imprinting, where half the gas is subjected to a phase change $\Delta\Phi$.

We focus here on a more asymmetric phase imprint with $\Delta\Phi = 130°$. This configuration is less well-studied experimentally, but it is of interest to us here because it creates faster-moving defects in the fluid, and more clearly reveals the full time evolution of the equilibration process.

Importantly, in this paper we demonstrate the generality of the induced defect structures and their dynamics within these two different perturbations. Our work establishes predictions for future experiments; we address experimentally accessible time scales and in our simulations we consider trapped gas parameters which match experimental capabilities. Finally, our work facilitates the more general understanding of the dominant equilibration pathways present in trapped atomic superfluids when they are perturbed.

In addition to suggesting directions for future experimental research, these studies yield further insight into related past experiments and simulations [1–6]. In the process we clarify the many different defect sequences which have been reported in the literature. Indeed, there has been significant controversy and debate over the characterization and decay processes of various defects, notably those associated with a phase imprint in which $\Delta\Phi \sim \pi$. There the original defect was thought to be a heavy soliton [5], later a vortex ring [7], and still later, as was consistent with predictions from some of our co-authors [8], established to be a solitonic vortex [6]. Similarly, defects formed via the Kibble-Zurek mechanism, using a temperature quench across the Bose-Einstein condensation (BEC) transition, were originally mis-identified as solitons [9] and later determined to be solitonic vortices [10]. It should be noted that while this earlier work [8] with $\Delta\Phi \sim \pi$ is a special case leading to anomalously long-lived defects, nevertheless, the earlier stages of equilibration in this case too, are addressed by the defect sequence we report here.

Among the earliest controlled perturbation experiments in cold gases [2] involved establishing propagating, localized depletions of density through a focused laser

beam. While these were designed to measure the speed of sound, these studies very early on elicited somewhat controversial [11] theoretical suggestions that dark solitons had been created in the process [3, 12–15]. Similar experiments have led to the observation of a variety of defects [1, 16–18], while other studies engineered localized excitations through phase imprinting [4–6, 19–21]. The theory associated with these experiments has suggested that solitons, or vortices or vortex rings (in some combination or sequentially) are created in the process [4, 6–8, 22–25].

The challenge presented by these perturbations has to do with how the superfluid system eventually eliminates or heals this planar defect as equilibration progresses. Quite generally we find that equilibration involves two types of processes. First, some equilibration processes will progressively extend the phase change $\Delta\phi$ over a larger volume, decreasing the maximum magnitude of the local phase gradient. Others will instead diminish the value of $\Delta\phi$ itself, minimizing the phase difference between the two sides. Facilitating these healing processes are vortex rings which repeatedly enter and exit the trap, and without which the overall sequence of equilibration cannot occur. We also report that the phase walls, which lead to vortex ring nucleation, tend to persist with (rather than convert to) vortex rings. In this paper we will show that all of these processes, which are to be associated with the planar nature of the initial defect, are in fact rather general.

In contrast to the commonalities upon which we focus here, past literature has suggested a wide variety of different defect evolutions. These include the report of a so-called oscillating soliton–vortex ring [1] created with a density depletion, while in a more complicated system of two density defects, there are claims of structures that involved both solitons and vortex rings [17]. Both phase imprinting and density depletions have led to reports of multiple solitons that bent significantly and in some cases decayed to vortices [16, 20]. Finally, numerical simulations of phase imprinting in very anisotropic traps led to the identification of a very weak vortex ring which rapidly moved away from the trap center [4]. Here we show how many of these defects are related, while a few arise due to different limits of trap geometry.

We focus on cigar-shaped traps which mirror those used in recent experiments [1, 6, 10]. These elongated traps, which are still well into the 3D regime, provide the advantage that one can study early-time dynamics without encountering reflections from trap edges. Furthermore, the cigar shape leads to significant and realistic inhomogeneity in the radial direction, which strongly influences defect behavior in these experimental systems. We will demonstrate that this inhomogeneity is, in fact, central for understanding most of the behavior seen here.

Our analysis is based on numerical simulations of the complex time-dependent Ginzburg-Landau (TDGL) equation for Fermi gases [26]. These studies address only the condensate dynamics and do not include the effects

of fermionic excitations. Considerable support for these numerics comes from previous related studies [8] of phase imprinting near $\Delta\Phi = \pi$ where most aspects of the experiments [6] confirmed the earlier predictions. In such simulations it is important to avoid artificially symmetric situations which unphysically stabilize long-lived defects. Here we include stochastic noise. The equation one solves is very similar to the Gross-Pitaevskii (GP) equation with the inclusion of dissipation. Thus, for the most part, our low dissipation results apply to the condensate dynamics in Bose gases as well.

II. OUR APPROACH

Our calculations are based on simulations of the wavefunction dynamics of a condensate in the Bardeen-Cooper-Schrieffer (BCS) to Bose-Einstein condensate (BEC) crossover, using an extension of TDGL to this crossover originally developed in Ref. [26]. Following Ref. [27] these authors derived the dynamical equation for the order parameter or gap Δ in the form

$$\left[a + b|\Delta(\boldsymbol{x},t)|^2 - \frac{c}{2m}\nabla^2 - id\frac{\partial}{\partial t} \right] \Delta(\boldsymbol{x},t) = 0 \qquad (1)$$

We work with the TDGL equation in a rescaled form [28],

$$e^{-i\theta}\partial_{\hat{t}}\hat{\Psi}(\hat{\boldsymbol{x}},\hat{t}) = \qquad\qquad (2)$$
$$\{[1 - \hat{V}(\hat{\boldsymbol{x}})] + \frac{1}{2}\hat{\nabla}^2 - |\hat{\Psi}(\hat{\boldsymbol{x}},\hat{t})|^2\}\hat{\Psi}(\hat{\boldsymbol{x}},\hat{t}) + \chi(\hat{\boldsymbol{x}},\hat{t}).$$

Time t, position $\boldsymbol{x}$, order parameter Δ and potential V have been converted to dimensionless normalized quantities,

$$\hat{t} = \frac{-a}{|d|}t, \quad \hat{\boldsymbol{x}} = \sqrt{\frac{-ma}{c}}\boldsymbol{x}, \quad \hat{\psi} = \sqrt{\frac{b}{-a}}\Delta, \quad \hat{V} = \frac{a_1}{-a}V. \tag{3}$$

With this, Eq. (1) reduces to Eq. (2), with $\theta = \pi/2 - \arg(d)$ and stochastic noise χ (discussed below) added.

Here θ controls the amount of dissipation, allowing us to move from the BCS ($\theta = 0$) regime to the BEC regime; for $\theta = \pi/2$ Eq. (2) reduces to the time-dependent GP equation [26, 29]. Work by one of the present authors shows that the inclusion of a gap in the fermionic spectrum stabilizes the pairs, making them rather long-lived [30]. As a result, we typically use $\theta = 88°$ in our simulations, and thus expect our results to also apply directly to BEC condensates [31].

In the weak coupling limit, sample parameters of $T_c = 70$ nK, $T/T_c = 0.7$, and coherence length $\xi = 3.2$ μm can be used with Ref. [26] to give the unit of $\hat{t}$ as 0.12 ms and the unit of $\hat{x}$ as 1.0 μm. The rescaled equation can similarly be obtained from the Gross-Pitaevskii equation [29] using the analogous transformations above. In this case, using pairs of ^{6}Li atoms with a chemical potential $\mu = k_B (120$ nK) (approximately equal to that reported in Ref. [5]) is sufficient to set the physical time and length
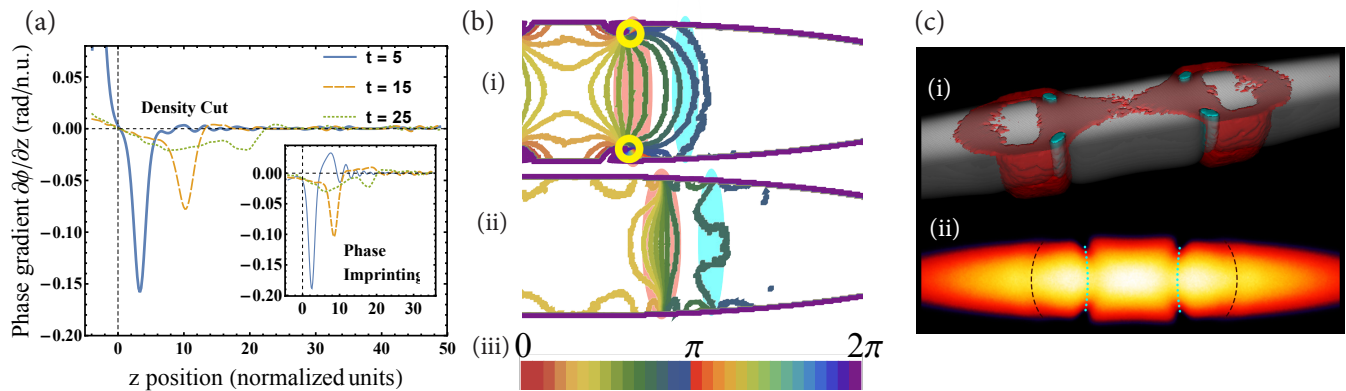
(a)

(b)

(c)

FIG. 1. (Color online) Figures illustrating the coexistence of a vortex ring and phase wall, along with the subsequent "tearing" process, in 3D simulations. (a) A plot of the gradient of the phase along the long axis (z-axis with $x = y = 0$), with data for both density cut and phase imprinting simulations at early times. It shows that in both density cut and phase imprinting perturbations, a sharp phase wall forms ($t = 5$). This is followed by the phase wall spreading out ($t = 15$) and finally by separating into a front phase wall and a vortex ring behind it, as shown by the two dips at $t = 25$. (b) Phase contour plots of $x = 0$ planes for two frames of the density cut simulation in (a), demonstrating the tearing process that occurs subsequent to the phase wall separation in (a). (b.i) Frame $t = 25$, which displays the system as the phase wall and vortex ring are "bending apart". (b.ii) Frame $t = 39$, displaying the system after tearing has occurred. Two separate phase walls now exist, one due to the original phase wall and the other due to the vortex ring. In this specific simulation, no vortices are present at the moment, but two are re-nucleated soon after this point. As shown in the legend (b.iii), $\pi/15$ contours of the phase are displayed. Thick circles (yellow), left ellipses (red), and right ellipses (cyan) highlight vortices, the vortex ring defect structure, and the original phase wall respectively. (c) Visualizations of the tearing process itself, showing the coexisting vortex ring and phase wall at $t = 32$ in the 3D density depletion simulation from (a) and (b). (c.i) 3D visualization of half the cloud (cut along the $y = 0$ plane). The main cloud shape (gray) is an isosurface of $|\Psi|^2$, which shows the volume inside which the superfluid density exceeds a low, but non-zero, threshold. The diffuse hourglass surface (red) illustrates the region of moderate density depletion from the equilibrium cloud, and the thin tubes (cyan) indicate the vortex rings (regions of large density depletion). (c.ii) Amplitude in the $x = 0$ plane from $|\Psi| = 0$ (black) to $|\Psi| = |\Psi_{\max}|$ (white). The dashed curves mark the front phase wall causing a density depletion, while the dotted cyan curves mark the location of the vortex ring. In all of (a-c), the "density cut" shows data after removing at $t = 0$ a Gaussian density depletion $V = Ae^{-z^2/(2\sigma^2)}$ with $A = 3.6$ and $\sigma = 0.71$. The phase imprinting shows data following a $130°$ phase imprinting at $t = 0$.

scales, namely a unit of $\hat{t}$ as 0.06 ms and a unit of $\hat{x}$ as 0.6 μm. More information can be found in the Supplementary Material of Ref. [8].

In this work we consider 2D and 3D anisotropic trapped Fermi gases subjected to either phase or density perturbations. The trap potential $\hat{V}$ in Eq. (2) is inserted by using the local density approximation, $\mu \rightarrow \mu - V(\boldsymbol{x})$, with the chemical potential μ rescaled to unity, so that $\hat{V}(\boldsymbol{x}) = \hbar(\omega_{\perp}^2(x^2 + y^2) + \omega_z z^2)/(2\mu)$. The function χ represents uniformly distributed thermal noise, and a fluctuation temperature can be set through $\langle \chi(\boldsymbol{x}, t)\chi^*(\boldsymbol{x}', t') \rangle = 2T_\chi \delta(\boldsymbol{x} - \boldsymbol{x}')\delta(t - t')$. We use a dimensionless fluctuation T_χ temperature very close to the zero-temperature limit (well below a nanokelvin for cold gas systems) [32]. We stress that the inclusion of noise in our numerical approach is a significant addition [8]. This avoids unphysical effects due to spatial symmetries present in many other simulations [3, 7, 24]. We note that some studies, even while breaking certain spatial symmetries, nevertheless maintain an unphysical reflection symmetry [24, 25].

Our work is based on numerical simulations discretized in up to 8192×1024 (2D) or 1024×256^2 (3D) grid points

and designed to solve Eq. (2) using a quasi-spectral split-step method.

III. SUPERFLUID PERTURBATIONS

For our simulations, we study a cigar-shaped trap with axial symmetry, typically taking $\gamma = \mu/(\hbar\omega_{\perp}) = 8.0$ and a trap ratio $\lambda = \omega_{\perp}/\omega_z = 6.6$ unless otherwise noted [33]. (For the sample weak coupling and GP parameters above, this corresponds to radial trapping frequencies of 160 Hz and 320 Hz, respectively.) In this regime the system is strongly under the influence of trap inhomogeneity, but well outside the 1D limit. Similar results for inhomogeneous, cylindrical traps are presented in App. C below. In the density depletion or "density cut" perturbation [1, 2] the superfluid equilibrates in the presence of a sharp barrier located about the $z = 0$ plane, physically corresponding to the application of a blue-detuned laser. This density cut is then removed suddenly, allowing the two sides of the cloud to interact.

Alternatively, we apply a "phase imprint" in which half of the cloud's phase is rotated by an angle $\Delta\Phi$. In contrast to recent experiments [5, 6] in which $\Delta\Phi \approx 180°$

was considered, here we focus on a less symmetric situation in which the phase difference is $\Delta\Phi = 130°$ and the defects evolve more rapidly. We note that the phase imprint technique has been frequently used to create solitary waves in superfluids [4–6, 19–21].

IV. DEFECT OVERVIEW

Figure 1 summarizes the major effects that we see in a 3D simulation. The general features we observe begin with the creation of a sharp phase gradient, either directly in phase imprinting or, as in a density depletion perturbation, through rapid movement of the superfluid. This "phase wall" moves and spreads out, then bends outward in its center, soon nucleating a vortex ring on the boundary. This process can be seen in Fig. 1(a), where one dip in the phase gradient splits into two dips at later times, one due to the front phase wall and the other due to the vortex ring.

Importantly, the front phase wall persists and bends forward after nucleation of the vortex ring. Eventually the phase wall and the vortex ring "tear" from each other, separating completely. This process can be seen in Fig. 1(b-c), where it is also accompanied by the ejection (and later, re-nucleation) of vortex rings.

These processes, as will be shown in subsequent simulations, are quite general. The bending of the phase wall causes vortex nucleation, and once vortices are nucleated, the "tearing" processes cause the initial phase wall to break up into multiple defects. We will next focus on more detailed analyses of these phenomena in 2D.

V. GENERAL DEFECT SEQUENCE

Figure 2 shows the evolution of vortex number for a sample of 2D simulations, also compared to the evolution of vortex number in the 3D runs of Fig. 1. The 2D simulations are quite consistent internally, and although the exact vortex number progression varies between 2D and 3D, all runs show similar perturbations in vortex number due to the tearing processes. In order to both explore this process more detail, and the generality of these effects under many different trap parameters, we now turn to a more microscopic analysis of 2D runs.

Figure 3 shows the evolution of the phase in the beginning moments of these simulations. Initially one sees a bending of the phase wall, which is a direct consequence of trap inhomogeneity. The phase wall is equivalent to a deformed dark soliton, which moves at a speed dependent on the phase change $\Delta\phi$ across it, as well as the local speed of sound. Due to the large central density, the speed of sound is highest at $(x, y) = 0$, and thus the phase wall moves fastest on the central axis [1, 34]. In contrast, the negligible density at the edge of the cloud effectively pins the phase wall on the boundary, establishing the dominant role of radial inhomogeneity.
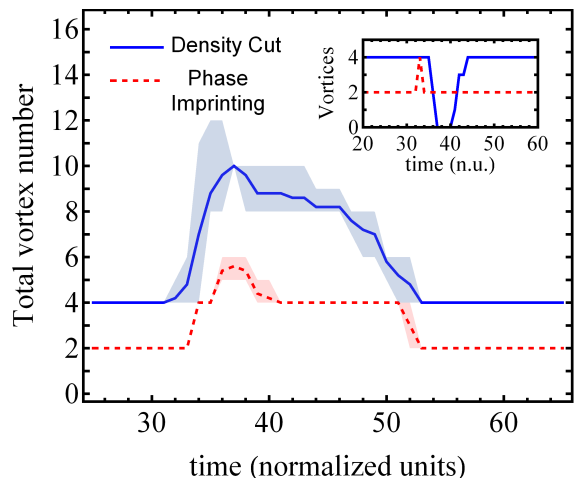

FIG. 2. (Color online) Plots of the total vortex number (irrespective of vortex orientation) vs. time for 2D simulations. Five runs with unique random noise were used for each perturbation. The curves show the mean vortex number, while the shaded regions about the curves show the full range of vortex numbers found at each timestep. This plot shows that density cuts and phase imprinting plots follow the same tearing process, first forming a vortex/antivortex pair (jump in vortex number near $t = 34$) and then ejecting the antivortices near $t = 38$. Finally, one of the remaining vortex pairs is ejected. Because density cuts produce vortices in both halves of the trap, all vortex numbers are doubled for it compared to phase imprinting. The inset shows vortex number for the two 3D runs in Fig. 1. Both exhibit a tearing process around $t = 35$, but because the vortex rings are close to the trap edge, the order of vortex ejection and nucleation differs somewhat – for a density cut, the original vortex ring exited before a new vortex ring entered, while for phase imprinting, the antivortices formed too close to the trap edge to be resolved in the measurements here.

This bending leads to the first step in the sequence shown in Fig. 3 which is the nucleation of a vortex pair at the boundaries (in 3D this corresponds to a vortex ring). The bent phase wall causes a strong superfluid flow toward the cloud center. This flow along the edge nucleates the vortex pair, and also pulls the vortex pair inward, as shown in the second frame of Fig. 3. This step has been observed previously in experiments [1] and simulations [3], and has been reported to play a crucial role in recent studies [5–8, 24, 25] [35].

Once nucleated, the vortices have multiple, dramatic effects on the system. Trap inhomogeneity and boundary effects [36] can be qualitatively associated with image vortices [8]. These cause the vortices to move toward the axial ends of the trap. The vortex cores themselves now form the radial edges of the phase wall, so these edges also now move axially outward rather than being pinned near the trap center along the axial direction. Simultaneously, the vortices also strongly influence the form of the phase gradient along the axis. The gradient is spread out axially while it simultaneously begins to
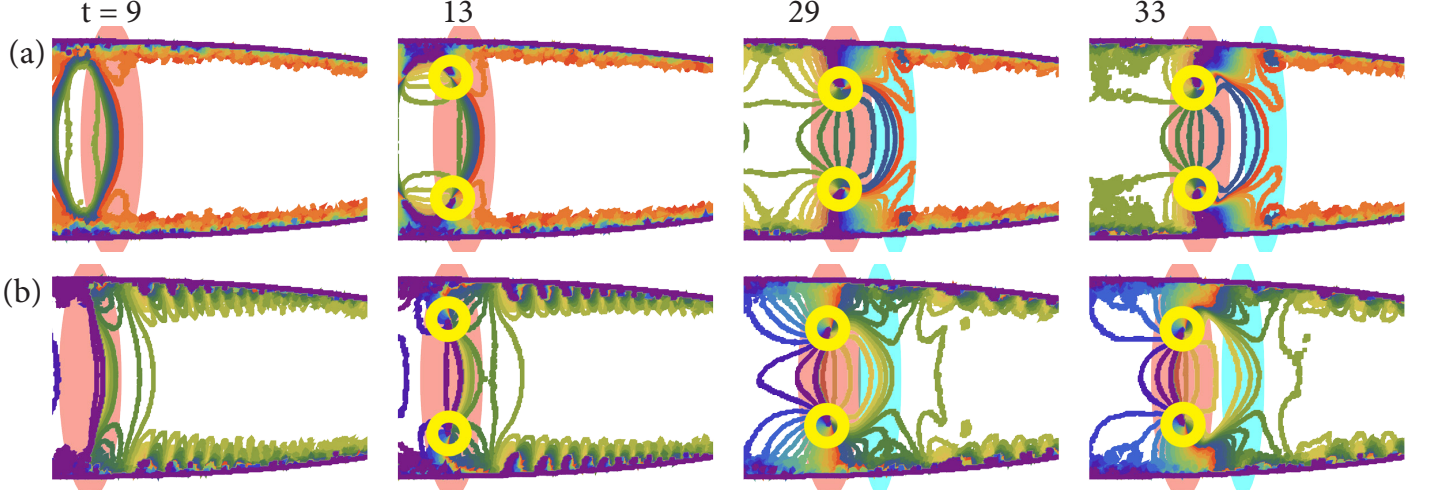
FIG. 3. (Color online) Phase contour plots of significant frames for the 2D (a) density cut and (b) phase imprinting runs, matching the parameters used for the simulations in Fig. 1, and using the same contours as Fig. 1(b). The right ellipses at $t = 29, 33$ (cyan) represent the phase wall that will "tear", while all other ellipses (red) represent the phase wall closer to the center. Vortices are indicated with thick circles (yellow). The first frame at $t = 9$ shows the initial bending of the phase wall, followed by the nucleation of the initial vortex pair at $t = 13$. The following frames show the beginning of the tearing processes, with a phase wall bending out from the vortex pair and its accompanying phase gradient.
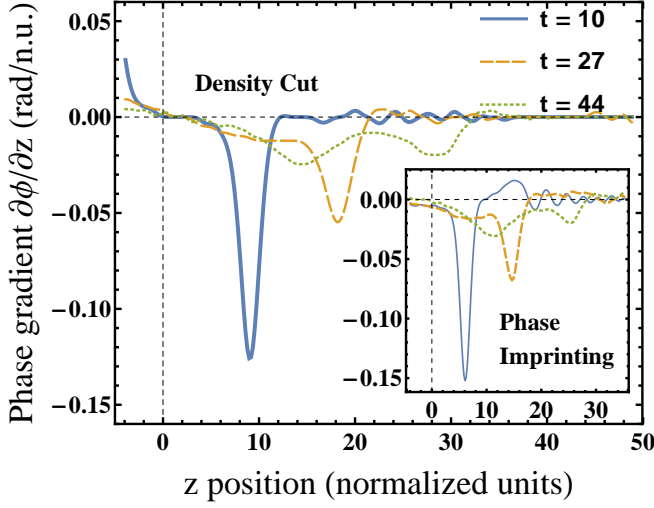

FIG. 4. (Color online) The evolution of the phase gradient along the axis of the trap for 2D simulations. The phase gradient starts out with a large, sharp dip, which later spreads out and then splits into two as the vortex pair and the original phase wall separate. As can be seen by comparing to Fig. 1(a), the timescales differ but the process of evolution matches very well for 2D and 3D simulations.

separate the original phase wall from the vortex pair (see Fig. 4).

A. Separation of phase wall and vortices

Importantly, these vortices do not destroy the original phase wall, but rather both defects coexist. After vortex nucleation (except in very one dimensional systems), the phase wall continues bending outwards, with its ends still formed by the vortices. This phase wall is necessarily weaker than before the vortex formation, due to the fact that a part of the initial phase change $\Delta\Phi$ now resides in the vortex pair structure itself, as shown in Fig. 4. (This phase wall can be distinguished as that local minimum of $d\phi/dz$ furthest from $z = 0$, as shown in Fig. 4.) However, it can be strong enough that, once the bending is severe, a second vortex pair nucleation occurs, as shown at $t = 35$ in Fig. 5 and observed in Fig. 2 [37]. This tearing process allows the phase wall to separate entirely from the initial pair of vortices. Often, the persistence of the original phase wall, and this tearing phenomenon, is robust enough that it occurs yet a second time.

A key part of the tearing process is the elimination of a vortex/antivortex pair on each side of the phase wall. Figure 6 shows this process in more detail, using the same simulations as Fig. 3. Figure 6(a) describes the tearing process from a density cut perturbation in which the phase wall bends outward, forming a beveled shape with its ends pinned by vortices. The beveling nucleates a vortex-antivortex pair near each phase wall end. In each quadrant, the original vortex annihilates with the antivortex of this new pair. This leaves a phase wall which bends and forms a new vortex resulting in two vortices in each quadrant. Figure 6(b) shows the same process from a 130° phase imprinting perturbation, but no pair annihilation occurs. Instead, the antivortex in the new
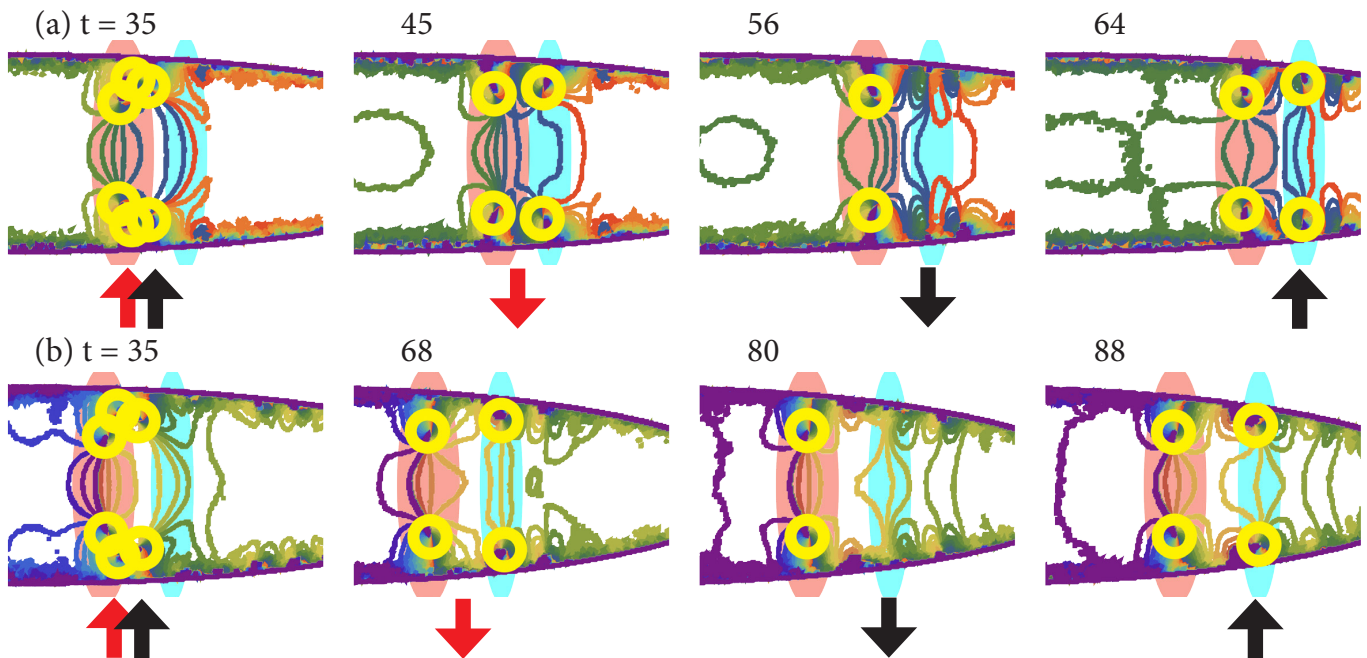
FIG. 5. (Color online) Phase contour plots of the simulations in Fig. 3 at later times. Here black (lighter red) arrows show vortices (antivortices) entering or leaving the cloud. The first frame at $t = 35$ shows the conclusion of the tearing process, with the nucleation of vortex-antivortex pairs and the separation of the two phase walls. The second frame [$t = 45$ in (a) and $t = 68$ in (b)] shows the loss of the antivortex, while the third frame shows the ejection of a vortex, followed by its renucleation in the final frame. Note that in (b), the final three frames show a portion of the cloud somewhat closer to the edge than all other frames.

pair is ejected. Both cases, however, result in the same two-vortex configuration in each quadrant, contributing to the generality both of this tearing process and of the future cloud evolution.

B. Vortex ejection and renucleation

The final general, dynamical feature is the repeated ejection and renucleation of at least some of the vortices. This is shown in the final three frames of the time sequence displayed in Fig. 5. We find that this process is driven by a specific dynamic mechanism: when the vortex pair forms, boundary effects cause the vortices to move rapidly toward the ends of the trap, while the center of the phase gradient between the vortex pair stays relatively stationary. This causes a "back-bending" of the phase wall, which changes the orientation of the superfluid velocity near the vortices, pointing partially out of the trap. This back-bending appears to eject the vortices from the trap. Once the vortices have left, the phase wall bends forward and renucleates new vortices driven by the same processes as described above.

C. Summary of results

The above steps are the general features of these inhomogeneous, trapped superfluids under two rather different perturbations. A few principles dictate most of this behavior: trap inhomogeneity causes phase walls to bend; bent phase walls nucleate vortex pairs and usually "tear" from the vortex pair; vortex pairs can later be ejected due to back-bending of phase walls. The differences between systems are differences in degree, such as multiple tearing processes, or vortex ejections and renucleations that differ in order and number. The number of such events is most closely related to the magnitude and steepness of the initial phase gradient induced by the perturbation.

Beyond the first 5 to 30 ms, in the later stages of equilibration, the behavior becomes more unique to each system, again depending strongly on the phase gradient applied. For large, sharp gradients the defects reach the end of the trap, causing a reflection that is dependent on the precise trap geometry, and can be much more complex and varied compared to the steps reported above [38]. For weaker phase gradients the defects dissipate or exit the trap before reflecting from the trap end, as explored further in App. B.
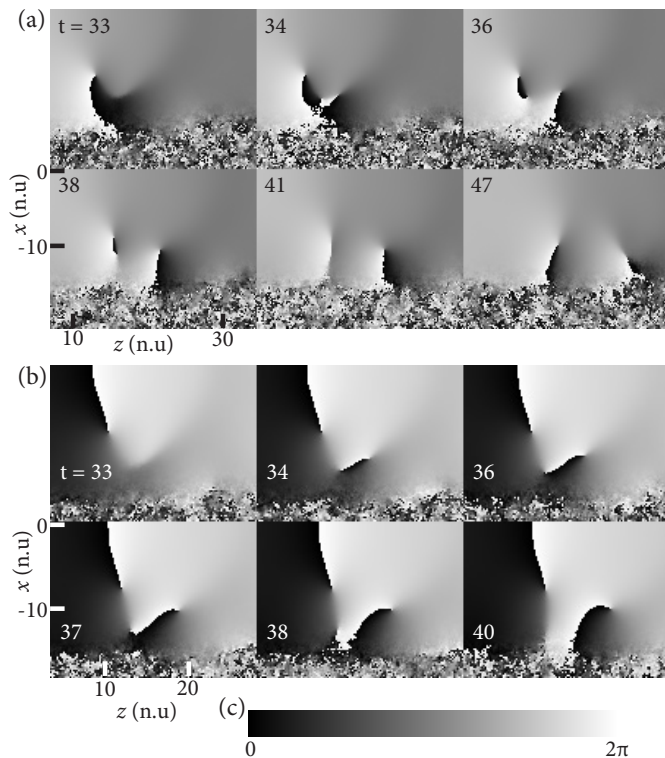
FIG. 6. Phase plots of tearing processes in the 2D simulations of Fig. 3, using the scale shown in (c). Here (a) is a density cut perturbation and (b) a phase imprinting perturbation, focused on the evolution of the bottom-right vortex and phase wall structure. In the first frame at $t = 33$ in both cases, a portion of the phase wall extends to the left and bottom. This strongly bent phase wall nucleates a new vortex-antivortex pair at $t = 34$. For (a), in the third and fourth frames ($t = 36$, 38), the antivortex moves close to the original vortex, annihilating and leaving a phase wall at $t = 41$. Finally, at $t = 47$ the phase wall nucleates a new vortex, leaving the observed two vortices described in the main text. For (b) and in contrast to (a), in the third, fourth and fifth frames the antivortex moves toward the trap edge, and is eventually ejected in at $t = 40$. This leads to the same end result as (a), but without the vortex pair annihilation observed in (a).

VI. TRAP DIMENSIONALITY EFFECTS

The above observations can be compared with earlier work, which investigated a similar sequence in a closer-to-1D configuration. That work was interpreted to be a ring–soliton oscillation [1]. We find that, instead, Ref. [1] exhibits the same dynamic mechanism described above, but with small changes due to the closer-to-1D configuration ($\gamma = 5.0$, $\lambda = 9$). In Ref. [1] the phase wall bends and nucleates a vortex ring as described in this work. However, the phase wall does not bend enough for part of it to survive and tear away from the vortex ring, so only one defect structure persists. This vortex ring can then undergo the dynamic ejection and renucleation process described above.

To make this comparison concrete, Figure 7 shows phase contour plots for a simulation run that displays an apparent oscillation between phase wall and vortices, very similar to Ref. [1]. Here a 130° phase imprinting perturbation has been applied. These 2D simulations have the same ω_z as other simulations presented in this work, but a trap ratio $\lambda = \omega_\perp/\omega_z = 13.2$, which moves the trap closer to a one-dimensional geometry ($\gamma = 4.0$), quite similar to Ref. [1]. This apparent oscillation is present in both density cut and phase imprinting perturbations.

As this process follows the same mechanism as that shown in earlier figures, which does not lead to oscillation, we view this as an extreme form of the dynamics described in the less-1D context presented above. We do not consider it to be a "Rabi" oscillation [1], which would imply an energetic near-degeneracy that allows an oscillation. Instead, this process is a consequence of non-equilibrium fluid dynamics of the superfluid – specifically the movement of vortices and phase walls in the very inhomogeneous trapping potential, which causes the phase wall to bend and the vortices to alternately be ejected and re-nucleated by the phase wall.

In the other limit of trap dimensionality, for very three-dimensional traps (large γ), the primary phenomena of the original phase wall bending forward and nucleating a pair of vortices is quite general, as is tearing for a wide range of γ values. However, at very large γ two major factors enter, as displayed in Fig. 8. First, the trap inhomogeneity is small, so the bending is much less pronounced, and tearing processes occur much later. Second, the reduced trap inhomogeneity and large size give freedom for many vortex-antivortex pairs to nucleate within the phase wall, making the system more chaotic. Especially for slow-moving phase walls (phase imprinting angles closer to 180°), these pairs were found to play a role in the dynamics for $\gamma \gtrsim 20$ with the parameters used here, with the largest values of γ producing the greatest number of pairs. These additional vortices also resemble those of Fig. 5 of Ref. [16], where $\gamma \sim 19$.

VII. CONCLUSION

In this paper, we have demonstrated general features in the evolution of planar defects in trapped superfluid gases. This common behavior is demonstrated by establishing the similarity in both phase imprinting and density depletion. This work focuses on the earliest stage of equilibration (at most about 30 ms), where these two perturbations lead to planar defects of a very similar fashion which are ultimately "healed" during the equilibration process. Later stages involve distinct phenomena, not discussed here, associated with trap boundaries and sometimes "solitonic" vortices [4, 6, 8, 10, 25, 39]. Not only do a variety of initial conditions or sudden perturbations produce these sharp phase walls, but once formed, they lead to a predictable set of rather complex dynamical processes accompanying superfluid equilibra-
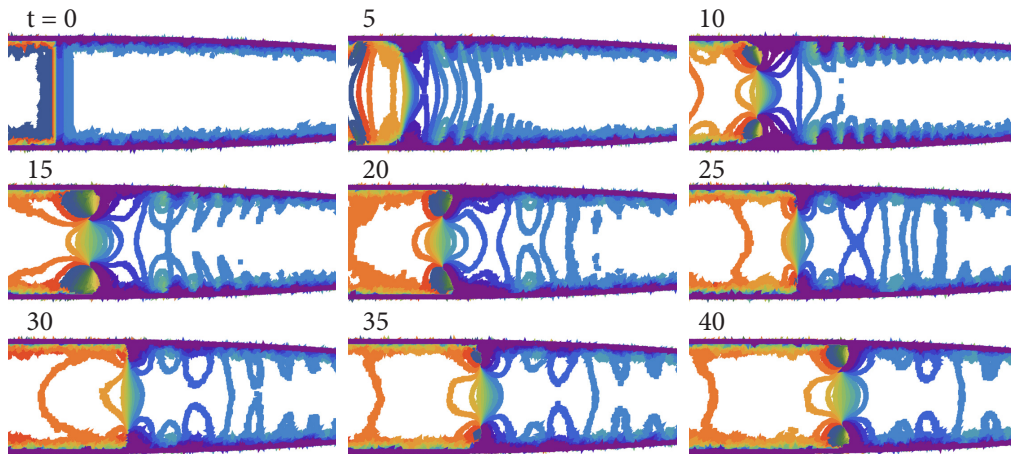
FIG. 7. (Color online) Contour plots of the phase for a trap which is more tightly confined radially ($\lambda = 13.2$). In this regime, the phase imprinting perturbation ($t = 0$) causes a phase wall to bend and nucleate a vortex pair ($t = 10$), as in the other simulations. In contrast to less-1D simulations, no "tearing" process can occur due to the additional confinement. Instead, the vortices propagate until they are later ejected, again leaving a phase wall ($t = 25$). This leads to another sequence of phase wall bending and subsequent vortex nucleation ($t = 35$). A second vortex ejection – phase wall – vortex nucleation sequence occurs but is not shown here.
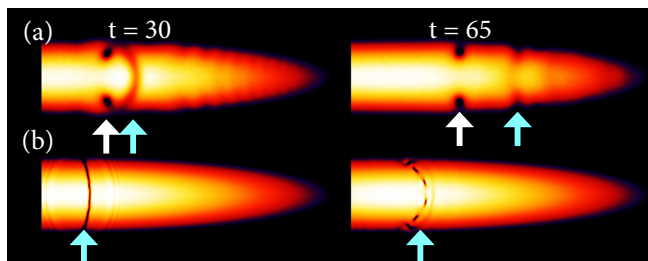

FIG. 8. (Color online) Plots comparing two different values of γ. In (a), the amplitude of the wavefunction is displayed at two time points for the same trap parameters as in Fig. 3(b) ($\gamma = 8$). In (b), a run with the same trap ratio λ, but much smaller $\omega_\perp$ and ω_z, is shown at the same time points ($\gamma = 32$). The first frames, at $t = 30$, demonstrate that the bending and "tearing" processes occur at very different timescales, due to the decreased local trap inhomogeneity. In the small trap, tearing is nearly complete; in the large trap, a vortex pair near the edge has not even formed yet. The large system is just beginning to tear at $t = 65$, while small system has a very well-separated vortex pair and phase wall. The $t = 65$ frame in (b) also demonstrates the other result of large traps: vortex-antivortex pairs form in the middle of the phase wall that is present, which quickly lead to much more chaotic dynamics. In both of these runs, a $150°$ phase imprinting was applied, which shows the vortex-antivortex creation more clearly than $130°$ at this system size. Cyan arrows indicate the initial phase wall, white arrows a separated vortex pair.

tion. This complexity, in turn, reflects the ability of planar defects to form multiple topological features.

The steps in common involve first a bending of the phase wall, next "tearing" that can create multiple vortex rings and/or phase walls, and finally vortex ejection and renucleation. These all serve to heal planar defects, and the formation and loss of vortex rings near the trap edge accompany and drive such healing processes. We emphasize that all of these dynamical processes are consequences of trap inhomogeneity and boundary effects, in contrast to other features, such as the snake instability, that may be seen in more homogeneous systems.

Finally, these predictions resulting from our simulations should be accessible experimentally and thus directly testable. The complete evolution of the planar defect, and especially the "tearing" process, should be observable. In addition, performing both phase imprinting and density cut perturbations would reveal the notable similarity in their effects. These simulations can thus serve as a guide for understanding defect evolution in a variety of future experiments.

Appendix A: Videos

Available in the Supplemental Material [40] are a selection of videos for different simulation runs. "Cut3D" and "PI3D" refer to the 3D density depletion and phase imprinting simulations of Fig. 1. "Cut2D" and "PI2D" show the runs in Fig. 3(a) and Fig. 3(b) of the main text, respectively. Finally, "Cyl" shows the density cut
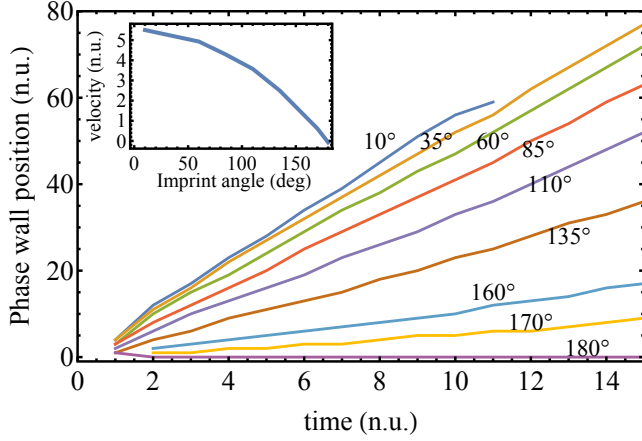
FIG. 9. (Color online) Plots of the position of the phase wall as a function of time, depending on the phase imprinting angle used, in terms of normalized units (n.u.). The phase wall position is calculated as the maximum magnitude of the phase gradient $\partial\phi/\partial z$ along the central z-axis, measuring from the trap center $z = 0$. The inset shows the calculated average velocity over this timescale, as a function of phase imprinting angle. Over this time scale, the phase imprinting angle dramatically changes the phase wall velocity. Only at the extremes of angles (see Table I for details), however, do the qualitative dynamics vary.

Angle	Vortices	Tearing	2nd Tearing	Re-nucleation	Tilting
10°					
35°					
60°	Y			U	
85°	Y	U		Y	
110°	Y	Y		Y	
135°	Y	Y	Y	Y	
160°	Y	Y		Y	Y
170°	Y	Y		Y	Y
180°	Y	N/A	N/A	N/A	N/A

TABLE I. Table of phenomena seen in defect evolution as the phase imprinting angle is varied. "Y" means the phenomenon is observed. "U" means it is uncertain, usually because the dynamics occur in a region of extremely low density. A traveling phase wall forms initially for all runs between 10° and 170°. For 180°, there is no traveling phase wall, and multiple vortices nucleate immediately. As a result, the system enters a much more chaotic state, and further phenomena cannot be identified. Here "tearing" is defined as a process in which one phase wall visibly separates into two phase walls; "2nd tearing" is seeing one of these phase walls again split into two. "Re-nucleation" means vortices are observed exiting the trap, and new vortices are later nucleated at a similar position.

simulation in Figs. 10(a) through 12(a).

All videos show the phase plot from 0 (black) to 2π (white) on the top half of the frame, and on the bottom half show the density (for 3D, density in the $x = 0$ plane), scaled from 0 (black) to a run-dependent maximum den-
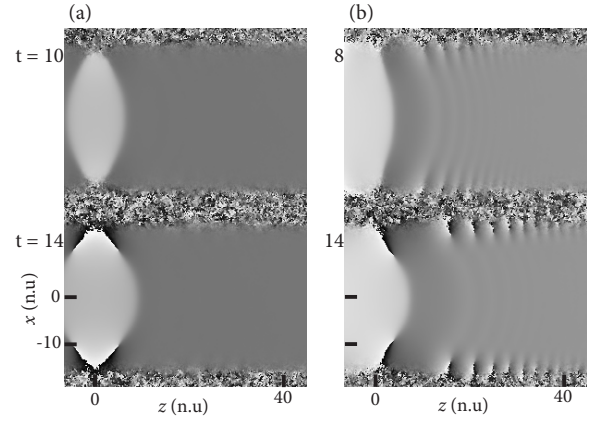

FIG. 10. Phase plots of (a) density cut and (b) 130° phase imprinting perturbations in an inhomogeneous, 2D cylindrical trap. Both simulations use a z-axis square well potential of inner length $\Delta z = 160$, and a radial trapping frequency of $\omega_\perp = 0.12\mu/\hbar$, giving a similar overall trap shape to the cigar trap in the main text. Shown here is the initial vortex pair creation resulting from the perturbation in both cases. For both perturbations, and just as in the case of the cigar trap, a phase wall forms and bends ($t = 10$ or 8), and the bending soon nucleates vortices that move inward ($t = 14$).

sity (white).

Appendix B: Variations of the phase imprinting angle

Figure 9 demonstrates the effect of changing the phase imprinting angle $\Delta\Phi$ that is applied in phase imprinting-type perturbations. In all cases, we find that the phase wall bends and begins to move outward. As noted in our earlier work [8], the phase imprinting angle does influence whether a vortex line will form, but it has little effect on the lifetime of the vortex ring. Here, Fig. 9 shows that the phase imprinting angle changes the velocity of the center of the phase wall. Qualitative differences only arise due to limits of the phase angle applied, as shown in Table I. At very small $\Delta\Phi < 60°$, not enough of a perturbation is applied to form vortices at all. At $\Delta\Phi \geq 160°$, the velocity of the phase wall is very small, so that the vortex pair tilts and one vortex is ejected. This situation was analyzed in Ref. [8]. Between these two limits, the behavior is quite general.

Appendix C: Cylindrical traps

Figures 10 through 12 characterize the defect sequence in an inhomogeneous cylindrical geometry. These defect sequences match very well with that described in the main text, which is due to the dominant influence of the radial inhomogeneity present in both systems. In these cylindrical traps, a strong square-well potential is ap-
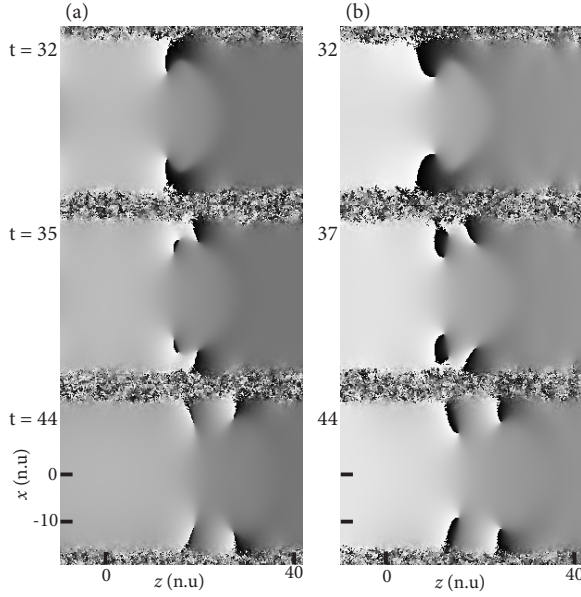
FIG. 11. Phase plots of a cylindrical trap for the same runs as Figure 10. Shown here is the tearing process that follows vortex pair nucleation. In the first frames of both (a) and (b), a phase wall bends outwards from the vortex pair that formed earlier. In the second frames, a vortex-antivortex pair is created on both the top and bottom of the system, and the antivortices proceed to (a) annihilate with the original vortices present in the system, or (b) rapidly exit the system. Finally, in the third frames two vortices of the same circulation are present along each edge. Again, these phenomena agree both between density cuts and phase imprinting, and between inhomogeneous cylindrical and cigar-shaped traps.

plied along the z-axis, while a harmonic trapping potential is used in the radial direction. Figures 10 through 12 display three characteristic parts of the defect sequence for both density cuts and phase imprinting, all of which match closely with the defect sequences described in the main text.

By contrast, for a "hard-walled" cylindrical trap, in which the potential in the $x-y$ plane is 0 inside a critical radius and very large outside that radius, the behavior is very different. This is due to the lack of inhomogeneity in the superfluid density. Instead, we observe only two defects: an extremely short-lived, small-radius vortex ring which nucleates then annihilates in the center, and vortices that nucleate right at the boundary but do not move inward or otherwise affect phase wall propagation. Both of these defects seem to carry very little energy, and have negligible effects on the dynamics. Other than these defects, no interesting evolution is observed – the phase walls simply travel towards the trap edges and slowly dissipate. When the phase walls reach the end, no defects remain (no reflections are present).

[1] I. Shomroni, E. Lahoud, S. Levy, and J. Steinhauer, "Evidence for an oscillating soliton/vortex ring by density engineering of a Bose-Einstein condensate," Nat. Phys. **5**, 193–197 (2009).

[2] M. R. Andrews, D. M. Kurn, H.-J. Miesner, D. S. Durfee, C. G. Townsend, S. Inouye, and W. Ketterle, "Propagation of sound in a Bose-Einstein condensate," Phys. Rev. Lett. **79**, 553–556 (1997).

[3] Janne Ruostekoski and Zachary Dutton, "Engineering vortex rings and systems for controlled studies of vortex interactions in Bose-Einstein condensates," Phys. Rev. A **72**, 063626 (2005).

[4] C. Becker, K. Sengstock, P. Schmelcher, P. G. Kevrekidis, and R. Carretero-González, "Inelastic collisions of solitary waves in anisotropic Bose-Einstein condensates: sling-shot events and expanding collision bubbles," New J. Phys. **15**, 113028 (2013).

[5] Tarik Yefsah, Ariel T. Sommer, Mark J. H. Ku, Lawrence W. Cheuk, Wenjie Ji, Waseem S. Bakr, and Martin W. Zwierlein, "Heavy solitons in a fermionic superfluid," Nature **499**, 426 (2013).

[6] Mark J. H. Ku, Wenjie Ji, Biswaroop Mukherjee, Elmer Guardado-Sanchez, Lawrence W. Cheuk, Tarik Yefsah, and Martin W. Zwierlein, "Motion of a solitonic vortex in the BEC-BCS crossover," Phys. Rev. Lett. **113**, 065301

(2014).

[7] Aurel Bulgac, Michael McNeil Forbes, Michelle M. Kelley, Kenneth J. Roche, and Gabriel Wlazlowski, "Quantized superfluid vortex rings in the unitary Fermi gas," Phys. Rev. Lett. **112**, 025301 (2014).

[8] Peter Scherpelz, Karmela Padavić, Adam Rançon, Andreas Glatz, Igor S. Aranson, and K. Levin, "Phase imprinting in equilibrating Fermi gases: The transience of vortex rings and other defects," Phys. Rev. Lett. **113**, 125301 (2014).

[9] Giacomo Lamporesi, Simone Donadello, Simone Serafini, Franco Dalfovo, and Gabriele Ferrari, "Spontaneous creation of Kibble-Zurek solitons in a Bose-Einstein condensate," Nat. Phys. **9**, 656–660 (2013).

[10] Simone Donadello, Simone Serafini, Marek Tylutki, Lev P. Pitaevskii, Franco Dalfovo, Giacomo Lamporesi, and Gabriele Ferrari, "Observation of solitonic vortices in Bose-Einstein condensates," Phys. Rev. Lett. **113**, 065302 (2014).

[11] Dan M. Stamper-Kurn, *Peeking and poking at a new quantum fluid: Studies of gaseous Bose-Einstein condensates in magnetic and optical traps*, Ph.D. thesis, Massachusetts Institute of Technology (1999).

[12] William P. Reinhardt and Charles W. Clark, "Soliton dynamics in the collisions of Bose - Einstein condensates:
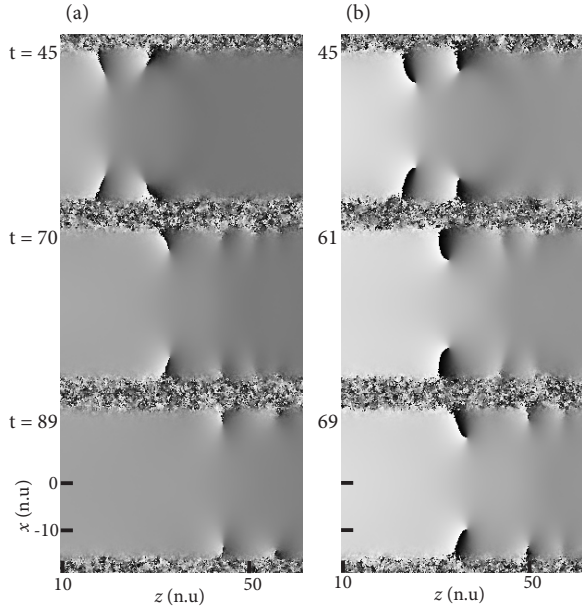
FIG. 12. Phase plots of a cylindrical trap for the same runs as Figure 10. These frames display the vortex exit and renucleation. In both (a) and (b), the front vortices are ejected in the second frame ($t = 70$ or 61), and renucleate, albeit very close to the boundary, in the third frame ($t = 89$ or 69). As before, these dynamics mirror those in cigar-shaped traps.

an analogue of the josephson effect," J. Phys. B **30**, L785 (1997).

[13] A. D. Jackson, G. M. Kavoulakis, and C. J. Pethick, "Solitary waves in clouds of Bose-Einstein condensed atoms," Phys. Rev. A **58**, 2417–2422 (1998).

[14] T. Hong, Y. Z. Wang, and Y. S. Huo, "Temporal dark solitons in nonuniform Bose-Einstein condensates," Phys. Rev. A **58**, 3128–3133 (1998).

[15] V. A. Brazhnyi and V. V. Konotop, "Evolution of a dark soliton in a parabolic potential: Application to Bose-Einstein condensates," Phys. Rev. A **68**, 043613 (2003).

[16] Zachary Dutton, Michael Budde, Christopher Slowe, and Lene Vestergaard Hau, "Observation of quantum shock waves created with ultra-compressed slow light pulses in a Bose-Einstein condensate," Science **293**, 663–668 (2001).

[17] Naomi S. Ginsberg, Joachim Brand, and Lene Vestergaard Hau, "Observation of hybrid soliton vortex-ring structures in Bose-Einstein condensates," Phys. Rev. Lett. **94**, 040403 (2005).

[18] A. Weller, J. P. Ronzheimer, C. Gross, J. Esteve, M. K. Oberthaler, D. J. Frantzeskakis, G. Theocharis, and P. G. Kevrekidis, "Experimental observation of oscillating and interacting matter wave dark solitons," Phys. Rev. Lett. **101**, 130401 (2008).

[19] S. Burger, K. Bongs, S. Dettmer, W. Ertmer, K. Sengstock, A. Sanpera, G. V. Shlyapnikov, and M. Lewenstein, "Dark solitons in Bose-Einstein condensates," Phys. Rev. Lett. **83**, 5198–5201 (1999).

[20] J. Denschlag, J. E. Simsarian, D. L. Feder, Charles W. Clark, L. A. Collins, J. Cubizolles, L. Deng, E. W. Hagley, K. Helmerson, W. P. Reinhardt, S. L. Rolston, B. I. Schneider, and W. D. Phillips, "Generating solitons by phase engineering of a Bose-Einstein condensate," Science **287**, 97–101 (2000).

[21] Christoph Becker, Simon Stellmer, Parvis Soltan-Panahi, Sören Dörscher, Mathis Baumert, Eva-Maria Richter, Jochen Kronjäger, Kai Bongs, and Klaus Sengstock, "Oscillations and interactions of dark and darkbright solitons in Bose-Einstein condensates," Nat. Phys. **4**, 496–501 (2008).

[22] A. Cetoli, J. Brand, R. G. Scott, F. Dalfovo, and L. P. Pitaevskii, "Snake instability of dark solitons in fermionic superfluids," Phys. Rev. A **88**, 043639 (2013).

[23] Wen Wen, Changqing Zhao, and Xiaodong Ma, "Dark-soliton dynamics and snake instability in superfluid Fermi gases trapped by an anisotropic harmonic potential," Phys. Rev. A **88**, 063621 (2013).

[24] Matthew D. Reichl and Erich J. Mueller, "Vortex ring dynamics in trapped Bose-Einstein condensates," Phys. Rev. A **88**, 053626 (2013).

[25] Gabriel Wlazlowski, Aurel Bulgac, Michael McNeil Forbes, and Kenneth J. Roche, "Life cycle of superfluid vortices and quantum turbulence in the unitary Fermi gas," arXiv:1404.1038.

[26] C. A. R. Sá de Melo, Mohit Randeria, and Jan R. Engelbrecht, "Crossover from BCS to Bose superconductivity: Transition temperature and time-dependent Ginzburg-Landau theory," Phys. Rev. Lett. **71**, 3202–3205 (1993).

[27] Elihu Abrahams and Toshihiko Tsuneto, "Time variation of the Ginzburg-Landau order parameter," Phys. Rev. **152**, 416–432 (1966).

[28] Igor S. Aranson and Lorenz Kramer, "The world of the complex Ginzburg-Landau equation," Rev. Mod. Phys. **74**, 99 (2002).

[29] Christopher Pethick and Henrik Smith, *Bose-Einstein Condensation in Dilute Gases*, 2nd ed. (Cambridge University Press, Cambridge, 2008).

[30] Jiri Maly, Boldizsár Jankó, and K. Levin, "Numerical studies of the s-wave pseudogap state and related T_c: the "pairing approximation" theory," Physica C **321**, 113–133 (1999).

[31] We see little variation in results for simulations with lower dissipation, $\theta = 89.5°$. Other dissipation effects mirror those shown in the Supplemental Material of Ref. [8].

[32] The temperature corresponds to $T_\chi = 5\times10^{-9}$. Note that this parameter includes a damping term γ_χ from atomic collisions, $T_\chi = \gamma_\chi T_{\mathrm{cloud}}$, which we approximate as 10^{-2} and is discussed elsewhere [41].

[33] In normalized units of Eq. (3), the Thomas-Fermi radii are $\hat{R}_\perp = \sqrt{2}\mu/\hbar\omega_\perp = \sqrt{2}\gamma$, $\hat{R}_z = \hat{R}_\perp\lambda$. The periods are $\hat{T}_\perp = 2\pi/\omega_\perp = 2\pi\gamma$ and $\hat{T}_z = \hat{T}_\perp\lambda$. For our commonly-used parameter set $\gamma = 8.0$ and $\lambda = 6.6$, this gives $R_z = 75$ and $T_z = 330$. The normalized units of Eq. (3) are used throughout the figures in this paper.

[34] N.G. Parker, N. P. Proukakis, and C.S. Adams, "Dark soliton dynamics in confined Bose-Einstein condensates," in *Focus on Soliton Research*, edited by L. V. Chen (Nova Publishers, 2006) pp. 1–49.

[35] The instability of solitons to vortex formation in trapped gases has also been modeled theoretically [39, 42, 43], though not necessarily in terms of the dynamic nucleation beginning at the boundary that is dominant here. We note that this nucleation at the boundary is related to but distinct from a true snake instability [22, 44–50],

which depends on transverse fluctuations of the soliton position and forms vortices within the soliton, not just at the boundary. As seen in Fig. 8, larger systems where trap inhomogeneity is less prominent can display both mechanisms of vortex formation [3, 16, 17, 34].

[36] Peter Mason and Natalia G. Berloff, "Motion of quantum vortices on inhomogeneous backgrounds," Phys. Rev. A **77**, 032107 (2008).

[37] A similar result of vortex ring formation with a persistent soliton was reported in Ref. [17]. Reference [3] also finds a second vortex/antivortex nucleation, but does not observe a second persistent feature form as we do.

[38] In this context, phase imprinting of $\Delta\Phi \approx 180°$ reflects a special case of a strong gradient creating a defect with very little velocity [8]. As described in our previous work and Table I here, the same initial sequence of phase wall bending and vortex ring nucleation is observed, but ultimately, because of the small defect velocity, an off-center ring results which leads to a longer-lived precessing line vortex [8].

[39] Joachim Brand and William P. Reinhardt, "Solitonic vortices and the fundamental modes of the snake instability: Possibility of observation in the gaseous Bose-Einstein condensate," Phys. Rev. A **65**, 043612 (2002).

[40] See Supplemental Material at [[URL]] or at http://oscon-scidac.org/projects/superfluids/defects for videos.

[41] Bogdan Damski and Wojciech H. Zurek, "Soliton creation during a Bose-Einstein condensation," Phys. Rev. Lett. **104**, 160404 (2010).

[42] S. Komineas and N. Papanicolaou, "Vortex rings and Lieb modes in a cylindrical Bose-Einstein condensate," Phys. Rev. Lett. **89**, 070402 (2002).

[43] S. Komineas and N. Papanicolaou, "Nonlinear waves in a cylindrical Bose-Einstein condensate," Phys. Rev. A **67**, 023615 (2003).

[44] E. A. Kuznetsov and S. K. Turitsyn, "Instability and collapse of solitons in media with a defocusing nonlinearity," Sov. Phys. JETP **67**, 1583–1588 (1988), originally Zh. Eksp. Teor. Fiz. 94, 119-129 (1988).

[45] A. V. Mamaev, M. Saffman, and A. A. Zozulya, "Propagation of dark stripe beams in nonlinear media: Snake instability and creation of optical vortices," Phys. Rev. Lett. **76**, 2262–2265 (1996).

[46] A. V. Mamaev, M. Saffman, D. Z. Anderson, and A. A. Zozulya, "Propagation of light beams in anisotropic nonlinear media: From symmetry breaking to spatial turbulence," Phys. Rev. A **54**, 870–879 (1996).

[47] Vladimir Tikhonenko, Jason Christou, Barry Luther-Davies, and Yuri S. Kivshar, "Observation of vortex solitons created by the instability of dark soliton stripes," Opt. Lett. **21**, 1129–1131 (1996).

[48] Yuri S. Kivshar and Barry Luther-Davies, "Dark optical solitons: physics and applications," Phys. Rep. **298**, 81–197 (1998).

[49] D. L. Feder, M. S. Pindzola, L. A. Collins, B. I. Schneider, and C. W. Clark, "Dark-soliton states of Bose-Einstein condensates in anisotropic traps," Phys. Rev. A **62**, 053606 (2000).

[50] B. P. Anderson, P. C. Haljan, C. A. Regal, D. L. Feder, L. A. Collins, C. W. Clark, and E. A. Cornell, "Watching dark solitons decay into vortex rings in a Bose-Einstein condensate," Phys. Rev. Lett. **86**, 2926–2929 (2001).